PERGAMON

International Journal of Solids and Structures 37 (2000) 5973–5994

INTERNATIONAL JOURNAL OF SOLIDS and STRUCTURES

www.elsevier.com/locate/ijsolstr

Edge effects in the failure of elastic/viscoelastic joints subjected to surface tractions

Z.Q. Qian, A.R. Akisanya*, M.S. Imbabi

Engineering Department, University of Aberdeen, King's College, Aberdeen AB24 3UE, UK

Received 10 March 1999; in revised form 23 August 1999

Abstract

The stress and displacement solutions are obtained for an elastic/viscoelastic joint subjected to a surface traction in the vicinity of an interface corner using elastic–viscoelastic correspondence principles and existing corresponding solutions for elastic/elastic joints. The intensity of the resulting stress singularity is determined by a combination of asymptotic analysis and the finite element method. A quasi-static assumption is used to investigate the effects of sliding and rolling contact loads near the interface corner on failure initiation. The results suggest the interface may experience stress reversal as the contact load (normal or shear) moves from one side of an interface corner to the other, leading to the possibility of fatigue failure. Further a relaxation or an increase of the interfacial stresses occurs depending on whether the edge load near the interface corner is on the elastic or viscoelastic side of the joint. The implications of the results in predicting the deformation and failure of asphalt concrete used in highway bridges are discussed.

Keywords: Stress singularity; Bonded joints; Failure initiation; Fatigue; Viscoelasticity

1. Introduction

It is well known that cracks initiate at the surface of brittle monolithic solids under rolling and/or sliding contacts because of the large tensile stress that exists near the surface (Suh, 1986). The magnitude of the tensile stress increases with increasing magnitude of the contact loads, and rapidly decreases with increasing distance away from the contact, suggesting a local effect. In this paper we examine the role of the near-surface stresses in the vicinity of an interface corner in controlling the initiation of failure in elastic/viscoelastic joints subjected to an edge traction. Here an interface corner is the intersection of the interface between bonded materials and the unbonded boundaries of the materials.

* Corresponding author. Tel.: +44-1224-272-989; fax: +44-1224-272-497.
E-mail address: a.r.akisanya@eng.abdn.ac.uk (A.R. Akisanya).

0020-7683/00/$ - see front matter
PII: S0020-7683(99)00247-4

Many modern engineering structures and components contain adhesively bonded and/or welded joints because they give a more uniform load distribution in comparison to other mechanical connectors. In some applications, the joints are subjected to surface traction resulting, for example, from contacts (sliding or rolling) with other components. Depending on the elastic and thermal properties of the bonded materials and the joint geometry, a stress singularity may develop at the interface corner. A detailed description of the different possible types of singularity at the interface corner of elastic bi-material wedges subjected to a surface traction has been given by Bogy (1970, 1971). One of the types of singularity is of the form $H r^{\lambda-1}$ $(0.5 \leq \lambda \leq 1)$ where r is the radial distance from the interface corner, H is the edge intensity factor and $(\lambda - 1)$ is the order of the stress singularity. λ depends on the material elastic properties and the joint geometry; typical values of λ are available in the literature, see for example Bogy (1970, 1971). The evaluation of the order of the stress singularity $(\lambda - 1)$ for elastic/elastic joints and its role in influencing failure initiation is now well established.

The magnitude of the intensity H depends on the material properties, the joint geometry and the magnitude of the applied load. The values of both H and λ are needed to fully describe the stress and displacement fields near the singular point. The need to develop an edge failure initiation criterion has led to recent interests in the evaluation of H for a number of joint geometries and load cases (Wang and Choi, 1982; Munz and Yang, 1992; Reedy, 1993; Akisanya and Fleck, 1997; Qian and Akisanya, 1999). Two different criteria have been proposed for the prediction of failure initiation at sharp wedges/notches and at interface corners. In the first criterion, failure initiation at interface corners or sharp notches, assuming small scale yielding near the corner, occurs when the magnitude of H attains a critical value (Gradin, 1982; Reedy, 1990; Qian and Akisanya, 1998a). The application of such a criterion has been hindered to some extent by the fact that the units of H are of the form (stress)(length)$^{1-\lambda}$, and hence depends on the local wedge angles and the elastic properties of bi-material joints.

Sih and Ho (1991) have proposed an alternative criterion where failure initiation occurs when the strain energy density at a point ahead of the notch attains a critical value. This criterion has been successfully used to predict the onset of failure and the initiation angle at the tip of notches in monolithic materials. Although the units of the strain energy density is independent of the wedge angle, the evaluation of the strain energy requires a knowledge of both H and λ, since both the stresses and the strains depend on these two parameters.

While the values of λ and H have been evaluated for a number of load cases and elastic/elastic joint geometries, similar analysis for elastic/viscoelastic joints has received relatively little attention. Many adhesives have viscoelastic properties and a significant number of bonded joints are used in elevated temperature applications where time-dependent deformation may occur in some of the materials. Since the mechanical properties of viscoelastic materials are time-dependent, the order of the singularity in elastic/viscoelastic and viscoelastic/viscoelastic joints is also time-dependent. Therefore, the relaxation of the edge stresses (at a constant applied strain) or the increase in deformation (at a constant applied load) in these material combinations will depend on the evolution of the order of the singularity and the intensity H.

Delale and Erdogan (1981) have shown that a relaxation of the edge shear stresses with increasing time occurs in an elastic/viscoelastic single lap joint subjected to a remote bending or transverse shear. Although the magnitude of the edge stresses are much higher than the magnitude of the corresponding stresses further away from the interface corner, no stress singularity was predicted because of the inherent plate theory assumptions in their analysis. Blanchard and Ghoniem (1989) extended the earlier singularity analysis for elastic/elastic joints presented by Bogy (1970, 1971) to viscoelastic materials. The order of the stress singularity and the edge intensity factor were determined as functions of time for viscoelastic/viscoelastic quarter planes (i.e. butt joints) subjected to a uniform change in temperature. The order of the singularity is independent of time when the two materials have identical relaxation times and time-independent Poisson's ratios.

More recently, Lee (1997, 1998) used Laplace transform technique together with the boundary element method to determine the order and intensity of the edge stress singularity for elastic/viscoelastic and rigid/viscoelastic quarter planes subjected to remote transverse tensile strain. By assuming a time-independent bulk modulus for the viscoelastic material, the analysis of the rigid/viscoelastic joint is significantly simplified since the solutions then depend only on the Poisson's ratio of the viscoelastic material. The analysis of the elastic/viscoelastic quarter plane, was also simplified by assuming a time-independent Poisson's ratio of the viscoelastic material (Lee, 1997). In both analyses, the intensity of the edge singularity was determined by comparing the interfacial stresses at a given time obtained from the numerical analysis with the corresponding asymptotic solution.

In this investigation, we determine the stress and displacement fields near the interface corner of an elastic/viscoelastic sandwiched joint subjected to edge traction in the vicinity of the interface corner. The stress and displacement solutions are obtained for cases where the edge traction (normal or shear) is applied only to one of the materials at any given time. The load is first applied to one of the materials in the vicinity of an interface corner while the other is left traction-free. Once the solutions to this particular load case have been obtained, the analysis is repeated with the load transferred to the material that was initially traction-free, while the originally loaded material is now traction-free. This quasi-static approach to the loading is used to examine the evolution of the edge stresses as the load moves from one side of the interface corner to the other, and therefore, mimics a sliding and/or rolling contact loading near the corner. The magnitude of the edge intensity factor H is determined as a function of time, edge loading and joint geometry.

Although the current analysis of the elastic/viscoelastic joint is different from that of Lee (1997), the results are complementary to those of Lee (1997). We have assumed a time-dependent Poisson's ratio of the viscoelastic material and the effects of the joint geometry have also been examined. In addition, the intensity of the singularity has been evaluated using an integral method, which has been shown by Qian and Akisanya (1998b) to be more accurate and relatively mesh insensitive compared to the method used by Lee (1997).

The structure of the rest of the paper is as follows. First, some essentials of the existing solutions for elastic/elastic joints are reviewed. We describe the joint geometry, material models and the analysis of the elastic/viscoelastic joint. The numerical method used in the present analysis is then discussed. The results are presented, and the solution of the interfacial stresses is used to explain the modes of failure observed in some industrially relevant elastic/viscoelastic joints.

2. The near-corner stress and displacement solutions for elastic/elastic joints

Consider a bonded joint consisting of two elastic, isotropic and homogeneous solids, identified as materials 1 and 2, as shown in Fig. 1. The intersection of the interface with the unbonded boundaries of the materials is referred to as the interface corner and denoted by A and B in Fig. 1. The mismatch of the elastic properties between the two materials are characterised by the Dundurs parameters α and β, which are defined for plane strain conditions by (Dundurs, 1969)

$$\alpha = \frac{\mu_1(1-\nu_2) - \mu_2(1-\nu_1)}{\mu_1(1-\nu_2) + \mu_2(1-\nu_1)}; \qquad \beta = \frac{\mu_1(1-2\nu_2) - \mu_2(1-2\nu_1)}{\mu_1(1-\nu_2) + \mu_2(1-\nu_1)} \tag{1}$$

where the subscripts denote the material number and, μ and ν are the shear modulus and Poisson's ratio, respectively.

A stress singularity may develop at the interface corners when the joint is subjected to mechanical or thermal loading. The stress and displacement fields near an interface corner, which are generally

obtained using either the complex variable method or the Airy's stress function approach, can be expressed as

$$\sigma_{ij}^{m} = H\, r^{\lambda-1} f_{ij}^{m} + \sigma^{*} f_{ijo}^{m}$$

$$u_{i}^{m} = \frac{1}{2\mu_{m}}\left[H\, r^{\lambda} g_{i}^{m} + \sigma^{*} r\, g_{io}^{m}\right] \tag{2}$$

where m (= 1, 2) is the material number; $(i, j) \equiv (r, \theta)$ are polar co-ordinates centred at the interface corner; $\lambda - 1$ is the order of the stress singularity; H is the edge intensity factor; f_{ij}, g_i, f_{ijo} and g_{io}, are the non-dimensional functions of the material parameters (α, β), polar co-ordinate θ and of the joint geometry; and σ^{*} is a characteristic measure of the applied load. The closed form expressions for the non-dimensional functions are available in the literature for a range of elastic/elastic joint geometries and loading; see, for example, Bogy (1970), Yang and Munz (1997), Akisanya and Fleck (1997) and Qian and Akisanya (1999). The second terms in Eq. (2) are the non-singular constant stress and the associated displacement; these functions vanish for remote mechanical loading and have finite values for uniform change in temperature (Munz et al., 1993) or local edge traction in the vicinity of the interface corner. The stress and displacement solutions in Eq. (2) must satisfy the continuity conditions at the interface (i.e. $\theta = \gamma$ and also the traction conditions near the interface corner, i.e. at $\theta = \pm\pi/2$.

The intensity of the singularity H is determined by combining the asymptotic solution in Eq. (2) with a numerical method like the finite element or the boundary element method. The magnitude of H depends on the details of the joint geometry, the material parameters (α, β) and on the magnitude of the applied loading. The order of the stress singularity is evaluated by solving a characteristic equation whose details depend on the joint geometry. For example, for a joint with an interface inclined at an angle γ to the x-axis as shown in Fig. 1, the characteristic equation is given by (Bogy, 1970; Qian and Akisanya, 1999)

$$\begin{aligned}
&\sin^{2}\lambda\pi + 2\left(2\lambda^{2}\cos^{2}\gamma - 1\right)\alpha \sin\lambda\pi \sin 2\lambda\gamma - 4\lambda^{2}\beta \sin\lambda\pi \sin 2\lambda\gamma \cos^{2}\gamma \\
&\quad + 4\lambda^{2}\cos^{2}\gamma\left(1 - \cos\lambda\pi \cos 2\lambda\gamma - 2\lambda^{2}\cos^{2}\gamma\right)\alpha\beta + \left[\sin^{2}2\lambda\gamma + 4\lambda^{2}\left(\lambda^{2} - 1\right)\cos^{2}\gamma - \lambda^{4}\sin^{2}2\gamma\right]\alpha^{2} \\
&\quad + \left[4\lambda^{2}\cos^{2}\gamma\left(\lambda^{2}\cos^{2}\gamma - 1 + \cos\lambda\pi \cos 2\lambda\gamma\right) + (\cos\lambda\pi - \cos 2\lambda\gamma)^{2}\right]\beta^{2} = 0
\end{aligned} \tag{3}$$

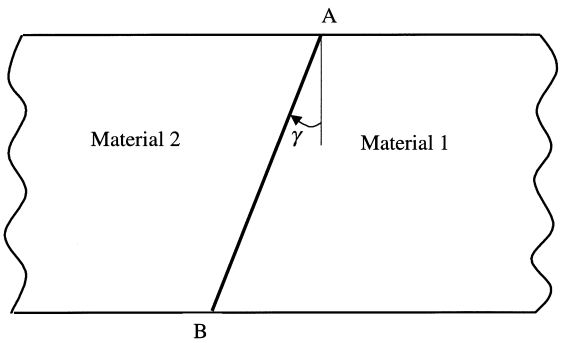

Fig. 1. A typical bi-material joint.

There may be more than one value of λ that satisfies Eq. (3). In this case each one will have its own associated intensity factor and, therefore, contribute to the edge field. λ may be real or complex, and the values of λ in the range $0 < \mathrm{Re}(\lambda) < 1$ result in a singularity of the form described by Eq. (2). For complex λ, the associated intensity H is also complex and the corresponding asymptotic expressions for the stresses and displacement are different from those given in Eq. (2). The stresses associated with complex λ alternate between negative and positive values very close to the singular point (Yang and Munz, 1995).

We shall make use of the elastic–viscoelastic correspondence principles and the solutions of the elastic/elastic joint described above to obtain the corresponding edge stress and displacement solutions for an elastic/viscoelastic joint subjected to edge tractions.

3. Formulation of the problem

3.1. Geometry

The joint geometry considered in this paper is shown in Fig. 2. It consists of a viscoelastic layer (material 2) sandwiched between two identical elastic solids (material 1). The joint is of length L and height h, where $L \gg h$. The interfaces between the elastic materials and the viscoelastic layer intersect the traction-free or the loaded surfaces of the bonded materials at interface corners A, B, C and D. Rectangular Cartesian (x, y) and plane polar co-ordinates (r, θ) placed at interface corner A are used to describe the stresses and the local geometry near the interface corner, as shown in Fig. 2(b). The interfaces are inclined at an angle γ with respect to the x-axis. Therefore, in the vicinity of an interface

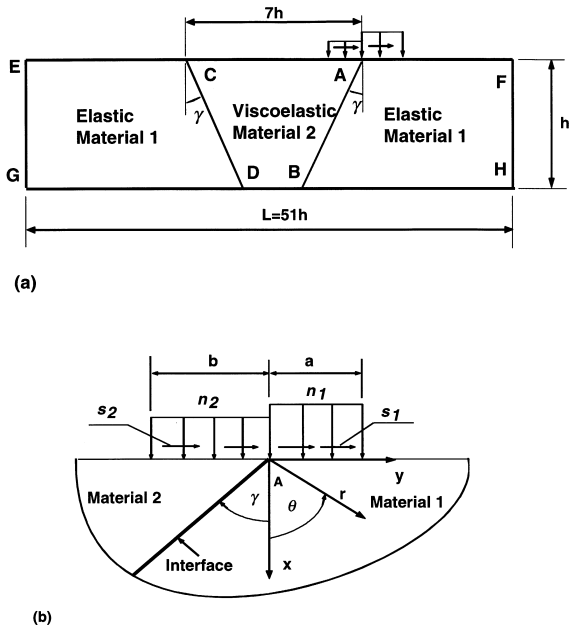

Fig. 2. (a) An elastic/viscoelastic joint geometry subjected to surface traction. (b) The details of the loading and local geometry near interface corner A.

corner, say A, the region $-\gamma < \theta \leq \pi/2$ is within the elastic material 1 while $-\pi/2 \leq \theta < -\gamma$ is within the viscoelastic material 2.

We assume in this analysis that the materials are perfectly bonded along the interfaces; the application of the results to the analysis of crack growth near the interface corner will be discussed later in the paper. For all the joint angles γ considered, the total length of the joint L is much greater than the smallest thickness of the viscoelastic layer DB, and DB $\gg h$. As such only one length scale in the geometry appears in the solutions, and that is the joint width h.

Without loss of generality, we consider only edge loading near interface corner A. The joint is subjected to one or a combination of the edge loading of magnitudes n_1, n_2, s_1, and s_2 in the vicinity of interface corner A as shown in Fig. 2(b). Here, n_1 and n_2 are the magnitudes of the uniform edge normal load on materials 1 and 2, respectively, while s_1 and s_2 are the corresponding magnitudes of the uniform edge shear load. The width of the loading on material 1 is denoted by a, and that on material 2 is denoted by b.

The joint geometry shown in Fig. 2 with $\gamma = 0$ is similar to that currently used in many asphaltic plug joints, where a composite mixture of rubberised bitumen and aggregates is sandwiched between concrete bridge decks in highway bridges. The bridge deck response is approximately elastic while that of the bitumen/aggregate mixture is viscoelastic. Asphaltic plug joints experience surface tractions resulting from the weight of the moving vehicles on the bridge. The results of the analysis to be presented in this paper will show that a better stress distribution and hence an increase in the service life of such joints can be obtained by appropriate selection of the joint angle.

3.2. Material model

We assume in the current analysis that material 1 is elastic, isotropic and homogeneous with the following time-independent material properties: shear modulus, μ_{1o}, bulk modulus K_{1o} and Poisson's ratio ν_{1o}. Only two of these three properties are independent. However, material 2 is assumed to be isotropic and *linear viscoelastic*. As such both strain and strain rates are infinitesimal, and the ratio of stress to strain is a function of time only and not of stress magnitude. Furthermore, with the exception of the viscoelastic stress–strain relations, which differ from those of the corresponding infinitesimal elasticity theory, all other governing equations follow directly from the theory of linear elasticity but with proper cognisance taken of the time-dependent nature of all the variables.

The stress–strain relation for the linear viscoelastic material 2, which is based on the principle that the effects of sequential changes in strains are additive, is of the form (Christensen, 1971)

$$\sigma_{ij}(t) = \int_{-\infty}^{t} \left\{ \mu_2(t-\tau) \left[\frac{\partial \varepsilon_{ij}}{\partial \tau} - \frac{1}{3}\delta_{ij} \frac{\partial \varepsilon_{kk}}{\partial \tau} \right] + \frac{3}{2} K_2(t-\tau) \left[\frac{1}{3}\delta_{ij} \frac{\partial \varepsilon_{kk}}{\partial \tau} \right] \right\} \mathrm{d}\tau \tag{4}$$

where the integration is carried out over all past times τ up to the current time t; δ_{ij} is the Kronecker delta, and $\mu_2(t)$ and $K_2(t)$ are the shear and volumetric relaxation moduli, respectively. In the current analysis we assume the solid shear relaxation modulus $\mu_2(t)$ is described by

$$\mu_2(t) = g_1 + g_2 \exp(-t/t_o) \tag{5}$$

where t_o is the relaxation time, and g_1 and g_2 are positive material constants. The shear relaxation function given by Eq. (5) is consistent with that for a Voigt model and a spring in series. For linear viscoelastic deformation where extremely small changes in volume occurs, the volumetric relaxation modulus is assumed to remain constant throughout the deformation, i.e

$$K_2(t) = K_{2o} \tag{6}$$

It is evident from Eq. (5) that

$$\mu_2(0) = g_1 + g_2$$

$$\mu_2(\infty) = g_1 \tag{7}$$

The evaluation of the time-dependent Poisson's ratio of the viscoelastic material $\nu_2(t)$ is discussed next.

3.3. Material elastic/viscoelastic mismatch parameters

The stress and displacement solutions near the interface corner A depend on the mismatch of the elastic and viscoelastic properties of the bonded materials. The governing equations for linear viscoelastic material can be obtained from the corresponding equations for elastic material by making use of the elastic–viscoelastic correspondence principles (Christensen, 1971). Here the variables in the equations for elastic solids (including the elastic constants) are replaced by the Laplace transform of the variables multiplied by the transform parameter. The equivalent viscoelastic equations in the time domain are then obtained by inverting the transforms. The time-dependent Dundurs' parameters have been obtained using this method.

The transformed material mismatch parameters $\bar{\alpha}(p)$ and $\bar{\beta}(p)$, where p is the Laplace transform parameter, are obtained by replacing the elastic constants in Eq. (1) with the Laplace transform of the corresponding parameter multiplied by p. Here and thereafter, a variable with overbar is the Laplace transform of the corresponding variable without overbar. For the elastic/viscoelastic joint under consideration, the transformed materials mismatch parameters $\bar{\alpha}(p)$ and $\bar{\beta}(p)$ are given by

$$\bar{\alpha}(p) = \frac{1}{p}\left[\frac{\mu_{1o}\left(1 - p\bar{\nu}_2(p)\right) - p\bar{\mu}_2(p)(1-\nu_{1o})}{\mu_{1o}\left(1 - p\bar{\nu}_2(p)\right) + p\bar{\mu}_2(p)(1-\nu_{1o})}\right]$$

$$\bar{\beta}(p) = \frac{1}{p}\left[\frac{\mu_{1o}\left(1 - 2p\bar{\nu}_2(p)\right) - p\bar{\mu}_2(p)(1-2\nu_{1o})}{\mu_{1o}\left(1 - p\bar{\nu}_2(p)\right) + p\bar{\mu}_2(p)(1-\nu_{1o})}\right] \tag{8}$$

where μ_{1o} and ν_{1o} are the time-independent shear modulus and Poisson's ratio of the elastic material 1, respectively and, $\bar{\mu}_2(p)$ and $\bar{\nu}_2(p)$ are the transformed shear relaxation modulus and Poisson's ratio of the viscoelastic material 2. It can be shown from Eqs. (5)–(7) and the standard elasticity equation relating Poisson's ratio to the shear and bulk moduli, that

$$\bar{\mu}_2(p) = \frac{p\mu_2(0) + \mu_2(\infty)/t_o}{p(p + 1/t_o)} \tag{9}$$

and

$$\bar{\nu}_2(p) = \frac{p\ t_o\left[3K_{2o} - 2\mu_2(0)\right] + \left[3K_{2o} - 2\mu_2(\infty)\right]}{2p^2 t_o\left[3K_{2o} + 2\mu_2(0)\right] + 2p\left[3K_{2o} + 2\mu_2(\infty)\right]} \tag{10}$$

The elastic–viscoelastic mismatch parameters and Poisson's ratio of the viscoelastic material in the time domain can now be obtained by inverting Eqs. (8) and (10). The closed form expressions for $\alpha(t)$, $\beta(t)$ and $\nu_2(t)$ are given in Appendix A.

The order of the singularity $(\lambda(t) - 1)$ for the elastic/viscoelastic joint is determined following similar elastic–viscoelastic correspondence principles described above. First the transformed characteristic

equation is obtained by replacing the elastic mismatch parameters α and β in Eq. (3) with the corresponding transformed parameters $\bar{\alpha}(p)$ and $\bar{\beta}(p)$, multiplied by p, and then inverting. The resulting characteristic equation in the time domain is given in Appendix B. The numerical solution of this transcendental equation gives the values of $\lambda(t)$. For some values of elastic and viscoelastic material constants there may be more than one value of $\lambda(t)$, and $\lambda(t)$ may even be complex. However, in this paper we have focused mainly on real values of $\lambda(t)$ and solutions have been obtained only for the smallest value of $\lambda(t)$ in the range $0 < \mathrm{Re}[\lambda(t)] < 1$.

4. The elastic/viscoelastic asymptotic solution

The asymptotic stress and displacement solutions near the interface corner of an elastic/elastic joint are given by Eq. (2). The determination of the solutions for elastic/viscoelastic joints by making use of the correspondence principles leads to very complicated expressions, and analytical inversion of the transforms may be very difficult. The asymptotic stress and displacement fields in the time domain for the elastic/viscoelastic joint geometry shown in Fig. 2 have been determined using the elastic–viscoelastic correspondence principles described in Section 3, the viscoelastic material behaviour given in Eqs. (5)–(7), and the solutions for elastic/elastic joints in Eq. (2). The asymptotic stress at a distance r from the interface corner A can be written as

$$\sigma_{ij}^{m}(t) = H(t) r^{\lambda(t)-1} F_{ij}^{m}(t) + \sigma^{*} F_{ijo}^{m}(t) \tag{11}$$

where, as before, m (= 1, 2) is the material number $(i, j) \equiv (r, \theta)$ are plane polar co-ordinates centred at the interface corner A in Fig. 2; and σ^{*} is a characteristic measure of the applied stress. For the joint geometry shown in Fig. 2, σ^{*} has a magnitude of n_1, n_2, s_1, or s_2 depending on which of the edge loads is applied. The first and second terms in Eq. (11) are the inverse of the corresponding transformed terms in Eq. (2). Numerical inversion using Jacobi polynomials (Miller and Guy, 1966) was used to obtain the first term in Eq. (11). This method does not require the evaluation of the transformed function in the complex p-plane. The analytical inversion of the transformed second term of Eq. (2) is complicated but not impossible; the term $\sigma^{*} F_{ijo}(t)$ obtained by analytically inverting the corresponding transform in Eq. (2) is given in Appendix C.

Both functions F_{ij} and F_{ijo} depend, in addition to the loading time t, on the elastic and viscoelastic constants (μ_{1o}, ν_{1o}, g_1, g_2, K_{2o}), the polar co-ordinates θ and the joint angle γ. The stress solutions given by Eq. (11) satisfy the stress continuity conditions at the interface ($\theta = \gamma$ and the traction boundary conditions at $\theta = \pm\pi/2$, at any time t. The only unknown parameter in Eq. (11) is the time-dependent edge intensity factor $H(t)$, which is defined such that $F_{\theta\theta}(t) = 1$ along the interface ($\theta = \gamma$), and is given by

$$H(t) = h^{1-\lambda}[n_1 \boldsymbol{a}_1 + n_2 \boldsymbol{a}_2 + s_1 \boldsymbol{a}_3 + s_2 \boldsymbol{a}_4] \tag{12}$$

where h is the joint width; n_1, n_2, s_1, and s_2 are the magnitudes of the edge loading (see Fig. 2(b)); and $\boldsymbol{a}_j$ ($j = 1, 4$) are the non-dimensional constant functions of time t, joint angle γ and the elastic and viscoelastic material constants (μ_{1o}, ν_{1o}, g_1, g_2, K_{2o}). The definition of $H(t)$ given by Eq. (12) suggests it must have units of (stress)(length)$^{1-\lambda}$. In the following section we describe how we have evaluated $H(t)$ for the joint geometry shown in Fig. 2 and representative values of the material constants (μ_{1o}, ν_{1o}, g_1, g_2, K_{2o}).

5. Numerical analysis

We evaluate the non-dimensional constants $\boldsymbol{a}_j$ ($j = 1, 4$) for each of the four load cases of the elastic/viscoelastic joint shown in Fig. 2, using a combination of a contour integral and the finite element method. This method, which is based on Betti's reciprocal law for viscoelastic solids (Christensen, 1971) and gives a path-independent integral, involves a convolution of the singular component of the asymptotic field (11) with a finite element solution. A full description of the evaluation of edge intensity factor for elastic/elastic joints using this method is available in Akisanya and Fleck (1997).

A detailed finite element analysis of the elastic/viscoelastic joint shown in Fig. 2 was performed using the ABAQUS (1997) finite element code. The joint height h was chosen as unity while the length of the joint was $L = 51h$. The largest thickness of the viscoelastic layer AC was kept at $7h$. However, the smallest thickness of the layer DB varied depending on the joint angle γ which had values of $\gamma = 0$, 15, 30 and 45°. The width of the loading was $a = b = h$. Plane strain conditions were assumed in the analysis. The geometry was discretised using eight-node quadrilateral isoparametric elements.

Numerical solutions were obtained for representative material properties based on the linear viscoelastic material model characterised by Eqs. (4)–(7). The linear viscoelastic material properties used in the analysis were $\mu_2(0) = 67.5$ GPa, $\mu_2(\infty) = 6.75$ GPa, $\nu_2(0) = 0.48$, and $\nu_2(\infty) = 0.498$, and $K_{2o} =$ 1665 GPa. The properties of the elastic material were, $\mu_{1o} = 338$ GPa and $\nu_{1o} = 0.33$. The volumetric relaxation modulus K_{2o} of the viscoelastic material was kept constant throughout the analysis. The normalised shear relaxation modulus, $\mu_2(t)/\mu_2(0)$, and Poisson's ratio, $\nu_2(t)$, of the viscoelastic material 2 are shown in Fig. 3(a) as a function of the normalised time t/t_o. We assume $t_o = 1$ min in the current analysis. The magnitude of $\mu_2(t)/\mu_2(0)$ decreases while $\nu_2(t)$ increases, with increasing normalised time.

The non-dimensional material parameters $\alpha(t)$ and $\beta(t)$ corresponding to the representative values of the material properties stated above were obtained using Eqs. (A2) and (A3); they are shown in Fig. 3(b). The magnitude of $\alpha(t)$ increases while that of $\beta(t)$ decreases with increasing normalised time t/t_o. Typical values of $\alpha(t)$ and $\beta(t)$ are: $[\alpha(0),\ \beta(0)] = [0.62,\ -0.016]$ and $[\alpha(10t_o),\ \beta(10t_o)] = [0.95,\ -0.002]$. We note, however, that the values of $\beta(t)$ for the typical elastic and viscoelastic properties considered here are quite small. There is, therefore, the temptation of assuming, $\beta = 0$ as is usually done under similar situation in interfacial fracture mechanics, where such assumption is used to avoid the complications associated with near-tip oscillating stress, with little or no effect on the interfacial stress intensity factor (Rice, 1988). However, such an approximation would be inappropriate in edge singularity analysis without any loss of accuracy since the material parameter β has a significant effect on the magnitude of both H and λ.

In the numerical analysis, solutions of the edge stresses are obtained for the edge loads n_1, n_2, s_1, and s_2 in the vicinity of interface corner A as shown in Fig. 2(b). The loads are applied statically one at a time. The magnitude of the applied load is then kept constant while the level of the resulting deformation is monitored; this is analogous to an indentation creep test. In the following we shall present the solutions for the edge intensity factor $H(t)$ and the corresponding evolution of stresses for each of the four load cases.

6. Results and discussion

6.1. Order of the stress singularity

The singular part of the stresses in the vicinity of the applied edge load for the joint geometry shown in Fig. 2 depend on the edge intensity factor $H(t)$ and the order of the singularity $(\lambda(t) - 1)$ as given by

Eq. (11). The order of singularity for the representative material properties obtained by using Eq. (B1) is shown in Fig. 4 for a range of joint angles γ.

As expected, joints with $\gamma = 0$ are more singular than those with $\gamma > 0$; the level of singularity decreases with increasing magnitude of γ. The value of $(\lambda(t) - 1)$ decreases with increasing time suggesting the stress field near the interface corner of the elastic/viscoelastic joint becomes more singular with increasing time. This is consistent with the evolution of the material parameter $\alpha(t)$ with time (see Fig. 3); the magnitude of $\alpha(t)$ increases with increasing loading time indicating an increase in the degree of mismatch in the elastic and the viscoelastic properties of the bonded materials.

The stresses near the interface corner of viscoelastic joints subjected to a constant remote transverse strain have been shown to relax (i.e. decrease in magnitude) with increasing time (Lee, 1998). In contrast, however, the increase in the level of stress singularity with increasing time observed for this creep-like loading might suggest an increase in the magnitude of the stresses in the vicinity of the load with increasing time. However, the effects of this observation on the magnitude of the stresses can only be quantified if the evolution of both $H(t)$ and $\lambda(t)$ is known, since the stresses depend, among other things, on the magnitude of these parameters.

We note also in Fig. 4 that the effect of the loading time on $\lambda(t)$ decreases with increasing magnitude of γ. The values of $\lambda(t)$ for $\gamma = 45^\circ$ are almost independent of time, they remain roughly constant with $\lambda(t) \approx 1$; the stress fields associated with $\lambda(t) \geq 1$ are non-singular.

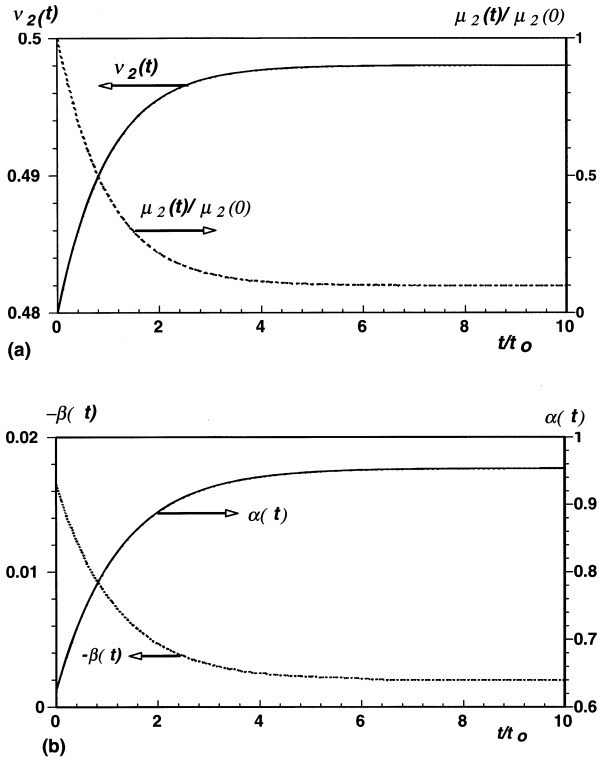

Fig. 3. (a) The normalised shear relaxation $\mu_2(t)/\mu(0)$ and Poisson's ratio $\nu_2(t)$ of the viscoelastic material 2 as a function of normalised time. (b) The elastic/viscoelastic material mismatch parameters $\alpha(t)$ and $\beta(t)$ as a function of time.

6.2. The edge intensity factor $H(t)$

The intensity $H(t)$ depends on the magnitude of the applied edge loads n_1, n_2, s_1, and s_2, and the joint geometry via the non-dimensional constants $\boldsymbol{a}_1$, $\boldsymbol{a}_2$, $\boldsymbol{a}_3$ and $\boldsymbol{a}_4$ as stated in Eq. (12). The values of these constants are shown in Fig. 5 for joint angles $\gamma = 0$, 15 and 30°. Recall that the non-dimensional constants $\boldsymbol{a}_1$ and $\boldsymbol{a}_2$ are associated with edge normal loads n_1, on the elastic material 1 and n_2 on the viscoelastic material 2, respectively. Similarly, $\boldsymbol{a}_3$ and $\boldsymbol{a}_4$ are associated with edge shear loads s_1 on the elastic material 1 and s_2 on the viscoelastic material 2, respectively.

For all the joint angles considered, the magnitudes of all of the non-dimensional constants decrease with increasing time; the rate of decrease is higher at small joint angles than at large joint angles. The effect of this on the magnitude of $H(t)$ and the edge stresses is not obvious, since they both depend on the time-dependent order of the stress singularity $[\lambda(t) - 1]$. The evolution of $[\lambda(t) - 1]$ shown in Fig. 4 suggests the edge stresses should become more singular (and hence increase in magnitude) as the loading time increases, while the evolution of each of the non-dimensional constants (Fig. 5) suggests a decrease in the magnitude of the stresses with increasing time. Therefore, the variation of the singular part of the edge stresses with time would be determined by the more dominant of these two competing effects. The magnitude of the total edge stress is, however, the sum of this singular part and the uniform constant stress field $\sigma^* F_{ijo}(t)$ (see Eq. (11)).

There are two important features of the results shown in Fig. 5. First, the magnitudes of the non-dimensional constant $\boldsymbol{a}_3$ and $\boldsymbol{a}_4$ associated with edge shear loads s_1 and s_2 are significantly greater than those of $\boldsymbol{a}_1$ and $\boldsymbol{a}_2$ which are associated with edge normal loads n_1 and n_2. This shows that the stresses resulting from the application of edge normal and shear loads of the same magnitude to one of the materials near the interface corner of an elastic/viscoelastic joint are dominated mainly by the shear load.

Secondly, the magnitudes of the constants associated with the loads on the elastic material 1 (i.e, a_1 and a_3) are much smaller than those associated with the loads on the softer viscoelastic material (i.e. a_2 and a_4). This is not surprising since the stiffer elastic material is expected to take a greater share of the load applied on it. Further, the non-dimensional constants $\boldsymbol{a}_1$ and $\boldsymbol{a}_4$ associated with normal load on the elastic material 1 and shear load on the viscoelastic material 2, respectively are negative while a_2 and a_3 associated with normal load on the viscoelastic material 2 and shear load on the elastic material 1 are positive. This shows that the singular component of the stresses near the interface corner undergoes a reversal as the edge load (normal or shear) is moved from one side of the corner to the other.

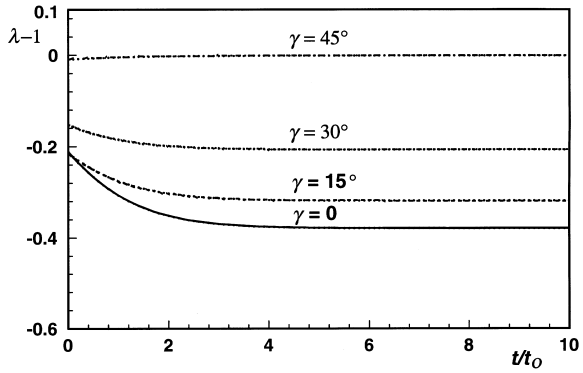

Fig. 4. The evolution of the order of the singularity $(\lambda(t) - 1)$ for the elastic/viscoelastic joint geometry.

6.3. Interfacial stresses near the loaded interface corner

The finite element solution of the total stress component $\sigma_{\theta\theta}(t)$ along the interface ($\theta = \gamma$) is shown in Fig. 6 as a function of the relative distance r/h from the interface corner A, for each of the four load cases. Here the stress is normalised by the magnitude of the appropriate edge load and the radial distance r is normalised by the joint height h. Recall that the total stress near the interface corner consists of two parts: a singular part characterised by $\lambda(t)$ and $H(t)$, and a uniform constant stress $\sigma^* F_{ijo}(t)$ where σ^* is the magnitude of the applied edge load and $F_{ijo}(t)$ are defined in Appendix C.

As expected, the magnitude of $\sigma_{\theta\theta}$ along the interface decreases with increasing joint angle γ, for all load cases. We note that the magnitude of $\sigma_{\theta\theta}$ along the interface relaxes (i.e. decreases with time) when the load (normal or shear) is applied to the elastic material 1 (see Fig. 6(a) and (c)). However, the interfacial stress component $\sigma_{\theta\theta}$ increases when the load is applied to the viscoelastic material 2 (Fig. 6(b) and (d)).

Let us first consider the situation where the load is applied on the viscoelastic material. The shear relaxation modulus of the viscoelastic material decreases with time as shown in Fig. 3. Consequently, the deformation of the viscoelastic material is expected to increase with time when a constant load is applied to it. The presence of the elastic material restricts the lateral deformation and prevents the free flow of the viscoelastic material, resulting in the development of a "back stress" at the interface. The magnitude of this stress should increase with time as the magnitude of lateral viscoelastic deformation to be restricted by the elastic material increases; this is consistent with the finite element solutions shown in Fig. 6(b) and (d).

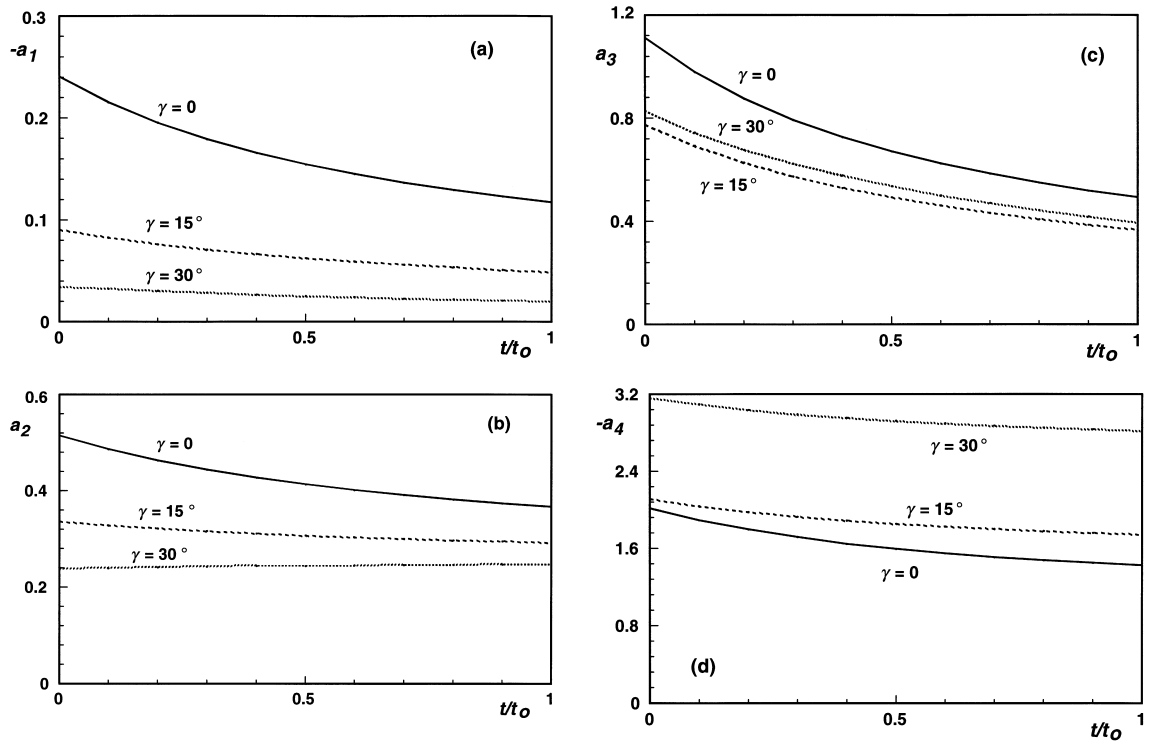

Fig. 5. The effects of joint angle γ, and loading time on the non-dimensional constants a_j ($j = 1, 4$) (a) a_1, (b) a_2, (c) a_3 and (d) a_4.

However, when the load is applied to the elastic material, the lateral deformation of the elastic material is small and does not change with time. Because the viscoelastic material is much "softer" than the elastic material, there is little or no restriction on the lateral deformation of the elastic material due to the presence of the viscoelastic material. Therefore, the magnitude of the interfacial stresses at the onset of loading $t/t_o = 0$ when the load is applied on the elastic material is expected to be lower than when the loading is applied on the viscoelastic material. This is consistent with the results shown in Fig. 6. Since the lateral deformation of the elastic material in this case does not change with time, the viscoelastic material is effectively subjected to a constant lateral strain at the interface between the two materials. This is equivalent to a relaxation test. The time-dependent deformation of the viscoelastic material, therefore, results in the relaxation of the interfacial stresses in order to maintain the constant level of lateral deformation in the elastic material, see Fig. 6(a) and (c).

Another observation from the finite element solutions of the interfacial stress component $\sigma_{\theta\theta}$ shown in Fig. 6 is that the stress changes sign as the edge load (normal or shear) is moved from one side of the interface corner to the other. This effectively subjects the interface to fatigue loading which may subsequently lead to fatigue failure in situations where the load moves from one side of the interface corner to the other, for example in rolling and sliding contacts.

The numerical results shown in Fig. 6 are for the individual load cases. If, however, the joint is subjected to a combination of any of these load cases or the applied load is changed after a given time has elapsed, the corresponding results can be obtained by making use of Boltzmann superposition

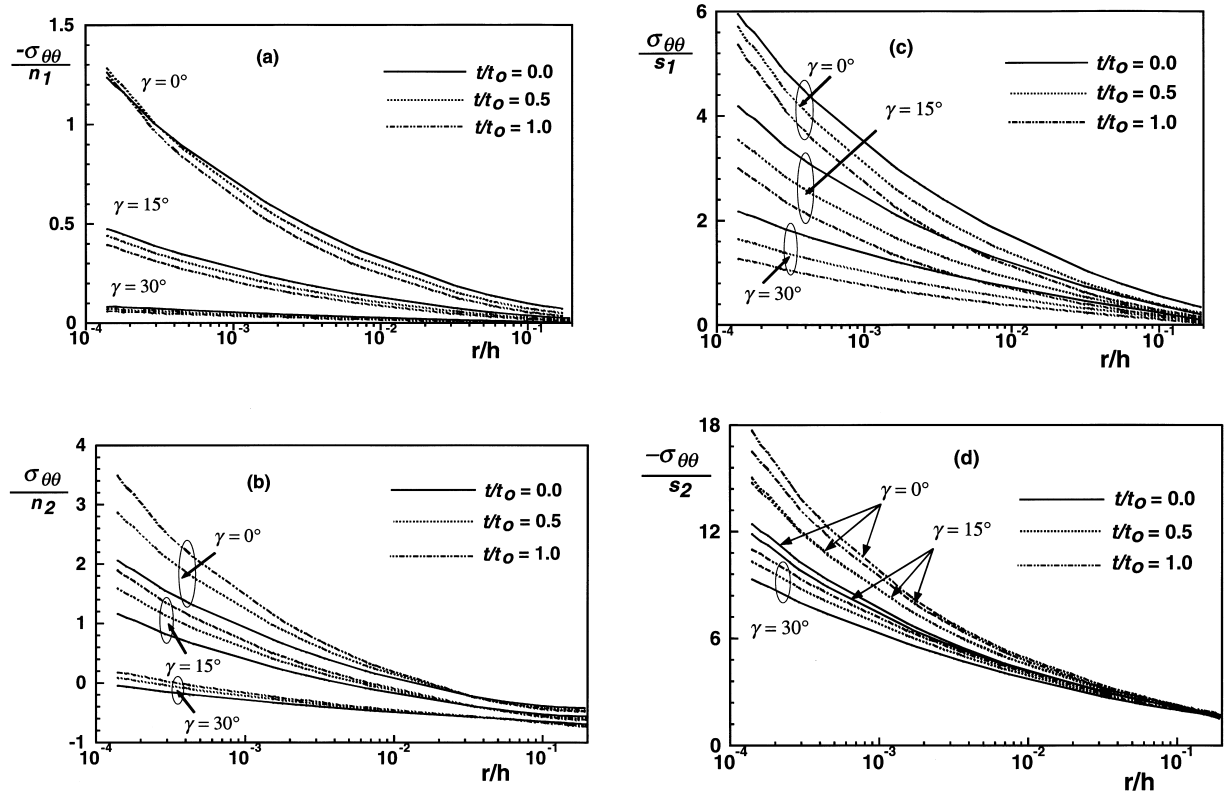

Fig. 6. The normalised interfacial stress component ($\sigma_{\theta\theta}/\sigma^*$ as a function of the normalised radial distance r/h and time t/t_o. Here h is the height of the joint and σ^* is the magnitude of the edge loading. (a) $\sigma^* = n_1$, (b) $\sigma^* = n_2$, (c) $\sigma^* = s_1$, and (d) $\sigma^* = s_2$.

principles (Christensen, 1971). A consequence of the Boltzmann superposition principles is that the deformation of a *linear viscoelastic* material is directly proportional to the applied stress when all the deformations are compared at equivalent time; the effect of different loads is additive. This is different from the conventional superposition procedures for infinitesimal deformation of a linear elastic material, because it takes account of the previous load (or deformation) history of the material, as reflected in the stress–strain relation of Eq. (4).

Interfacial fracture and crack growth are controlled by the ratio of shear stress to the normal stress along the interface. The increasing magnitude of the shear stress increases the likelihood of edge debonding in bonded joints and delamination in laminated composites. The ratio of the interfacial shear stress σ_{r_θ} to the normal stress $\sigma_{\theta\theta}$ for the elastic/viscoelastic joint geometry under consideration is shown in Fig. 7, for each of the four load cases. When the load is on the elastic material 1 (i.e. Fig. 7(a) and (c)) the stress ratio is negative with a magnitude which remains approximately constant up to a distance $r = 0.01h$, after which the magnitude decreases rapidly with increasing distance from the interface corner. As expected the magnitude of the stress ratio increases with increasing joint angle γ.

The results of the stress ratio $(\sigma_{r_\theta}/\sigma_{\theta\theta})$ when the load is on the linear viscoelastic material 2 are shown in Fig. 7(b) and (d). For normal load n_2, the magnitude of the stress ratio for $\gamma = 30^\circ$ decreases monotonically with increasing distance from the interface corner while that for $\gamma = 0$ and 15° increases initially up to a distance $r = 0.01h$, after which the stress ratio changes sign and subsequently decreases in magnitude with distance. However, the magnitude of the stress ratio for a shear load s_2 on the viscoelastic material (Fig. 7(d)) decreases with increasing distance from the interface corner.

It is important to point out that the results shown in Fig. 7 are the interfacial stress ratio $(\sigma_{r_\theta}/\sigma_{\theta\theta})$ near the interface corner in the absence of any edge crack. The results can, therefore, be used in conjunction with an appropriate failure criterion to assess the likelihood of failure initiation. Stress redistribution will occur upon the initiation of an edge crack, and the magnitude of the stress ratio ahead of the crack may be different from those shown in Fig. 7.

7. Application to joint design and failure

One of the main objectives in the design of bonded joints is to minimise the edge stresses. This can be accomplished by choosing either the materials and joint geometry which ensure the magnitude of λ is very close to, or greater than 1; or the magnitude of the applied load and the joint geometry which minimises the magnitude of the intensity H. It is however difficult, if not impossible, to completely eliminate stress singularities in bonded joints and sandwich structures, especially for elastic/viscoelastic joints where the values of both λ and H change with time. Therefore, in the design of such joints, the evolution of both λ and H over the duration of loading (as determined in this paper) needs to be considered before deciding on which joint geometry or loading satisfies the objectives stated above.

There are limited experimental data to support the idea that failure initiates at an interface corner when the magnitude of intensity H attains a critical value. This critical value is generally determined by experiments (see for example, Fett, 1996; Qian and Akisanya, 1998a), but requires an appropriate calibration for H as determined in this paper for elastic/viscoelastic joints. Once such failure occurs and the size of the crack is much smaller than the extent of the elastic edge singularity, the growth of the crack is controlled by the magnitude of the intensity H of the edge singularity. The coupling between the crack tip stress intensity factors for edge cracks embedded within an edge singularity and the intensity H of the singularity has been obtained by Akisanya and Fleck (1997) for elastic/elastic butt joints and by Liu and Fleck (1998) for elastic/elastic scarf joints. These solutions can be applied to the elastic/viscoelastic joint under investigation and used to determine the evolution of the crack tip stress intensity factor with time for a short crack near the interface corner.

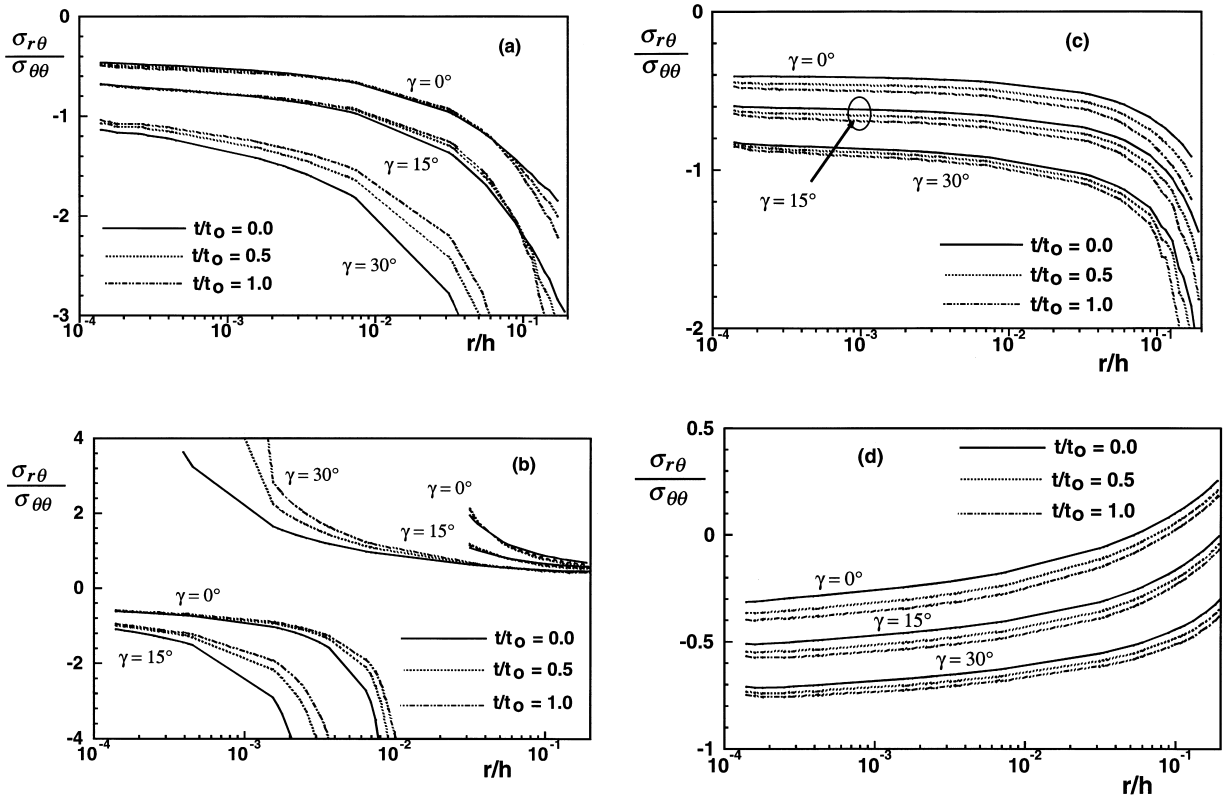

Fig. 7. The ratio of shear to normal stress ($\sigma_{r\theta}/\sigma_{\theta\theta}$) at the interface as a function of the relative distance from the interface corner r/h, and normalised loading time t/t_o, for (a) normal load n_1, (b) shear load s_1, (c) normal load n_2 and (d) shear load s_2.

We have shown earlier that the alternation of the edge loading between the two bonded materials results in interfacial stress reversal and the possibility of fatigue failure. The continuous growth of such failure, if it occurs, depends on the properties of the materials including the toughness of the interface. For elastic/viscoelastic joints subjected to cyclic alternation of edge loading between the bonded materials as in asphaltic plug joints used in highway bridges, the progressive accumulation of deformation in the viscoelastic material may actually result in the healing of the fatigue crack at moderate temperatures. However, at very low temperatures when the viscoelastic material behaves more like an elastic brittle material, progressive fatigue crack propagation near the edge may occur. The range and mean of the alternating stress can be significantly reduced by appropriate choice of the joint angle γ.

8. Conclusions

The stress field near the interface corner of an elastic/viscoelastic joint subjected to edge traction in the vicinity of the corner has been determined using elastic–viscoelastic correspondence principles. A linear viscoelastic material model is assumed and a combination of asymptotic analysis and the finite element solutions was used to obtain the stresses near the loading. The time-dependent stresses near the interface corner where the load is applied has been shown to be of the form

$\sigma_{ij}(t) = H(t)r^{\lambda-1}F_{ij}(t) + \sigma^* F_{ijo}(t)$, where r is the radial distance from the corner and σ^* is a measure of the applied load. The solutions of the intensity $H(t)$, order of stress singularity $\lambda(t)-1$ and the non-dimensional function $F_{ijo}(t)$ have been presented in the paper for a range of joint angles and normal and shear edge loadings.

The numerical results show that a large stress gradient exists near the loaded interface corner. Further, the magnitude of the interfacial stress component $\sigma_{\theta\theta}$ near the loaded edge increases with time if the loading is on the viscoelastic material, while it decreases with time (i.e. relaxes) if the loading is on the elastic material. The movement of the edge loading from one side of the interface corner to the other, which is typical of sliding and rolling contacts, subjects the interface to a stress reversal and, therefore, increases the possibility of failure by fatigue.

Acknowledgements

The authors are grateful for helpful discussions with Profs. N.A. Fleck and H.W. Chandler, and for financial support from the Engineering and Physical Sciences Research Council, UK.

Appendix A

Poisson's ratio of the viscoelastic material 2 in the time domain obtained by analytically inverting the corresponding transform in Eq. (10) is given by

$$\nu_2(t) = \frac{3K_{2o} - 2\mu_2(\infty)}{6K_{2o} + 2\mu_2(\infty)} + \left[\frac{3K_{2o} - 2\mu_2(0)}{6K_{2o} + 2\mu_2(0)} - \frac{3K_{2o} - 2\mu_2(\infty)}{6K_{2o} + 2\mu_2(\infty)}\right] \exp\left(-q\frac{t}{t_o}\right) \tag{A1}$$

where

$$q = \frac{3K_{2o} + \mu(\infty)}{3K_{2o} + \mu(0)}$$

The elastic/viscoelastic materials mismatch parameters $\alpha(t)$ and $\beta(t)$ in the time domain are given by

$$\alpha(t) = \frac{c_2}{c_1} + \frac{d_2\chi_1^2 + b_2\chi_1 + c_2}{\chi_1(2d_1\chi_1 + b_1)} \exp(-\chi_1 t) + \frac{d_2\chi_2^2 + b_2\chi_2 + c_2}{\chi_2(2d_1\chi_2 + b_1)} \exp(-\chi_2 t) \tag{A2}$$

$$\beta(t) = \frac{c_3}{c_1} + \frac{d_3\chi_1^2 + b_3\chi_1 + c_3}{\chi_1(2d_1\chi_1 + b_1)} \exp(-\chi_1 t) + \frac{d_3\chi_2^2 + b_3\chi_2 + c_3}{\chi_2(2d_1\chi_2 + b_1)} \exp(-\chi_2 t) \tag{A3}$$

where

$$b_1 = \frac{1}{t_o}\left\{2\mu_{1o}\left[3K_{2o} + 2\mu_2(0) + 2\mu_2(\infty)\right] + 2(1-\nu_{1o})\mu_2(\infty)\left[3K_{2o} + 2\mu_2(0)\right] + 6(1-\nu_{1o})K_{2o}\mu_2(0)\right\} \tag{A4}$$

$$b_2 = \frac{1}{t_o}\left\{2\mu_{1o}\left[3K_{2o} + 2\mu_2(0) + 2\mu_2(\infty)\right] - 2(1-\nu_{1o})\mu_2(\infty)\left[3K_{2o} + 2\mu_2(0)\right] - 6(1-\nu_{1o})K_{2o}\mu_2(0)\right\} \tag{A5}$$

$$b_3 = \frac{1}{t_o}\{\mu_2(\infty)[3\mu_{1o} - (1-2\nu_{1o})(3K_{2o} + 2\mu_2(0))] + 3K_{2o}\mu_2(0)\} \tag{A6}$$

$$c_1 = \frac{1}{t_o^2}\{\mu_{1o}[3K_{2o} + 4\mu_2(\infty)] + 2(1-\nu_{1o})\mu_2(\infty)[3K_{2o} + \mu_2(\infty)]\} \tag{A7}$$

$$c_2 = \frac{1}{t_o^2}\{\mu_{1o}[3K_{2o} + 4\mu_2(\infty)] - 2(1-\nu_{1o})\mu_2(\infty)[3K_{2o} + \mu_2(\infty)]\} \tag{A8}$$

$$c_3 = \frac{\mu_2(\infty)}{t_o^2}\{3\mu_{1o} - (1-2\nu_{1o})[3K_{2o} + \mu_2(\infty)]\} \tag{A9}$$

$$d_1 = \mu_{1o}[3K_{2o} + 4\mu_2(0)] + 2\mu_2(0)(1-\nu_{1o})[3K_{2o} + \mu_2(0)] \tag{A10}$$

$$d_2 = \mu_{1o}(3K_{2o} + 4\mu_2(0)) - 2\mu_2(0)(1-\nu_{1o})(3K_2 + \mu_2(0)) \tag{A12}$$

$$d_3 = 3\mu_{1o}\mu_2(0) - (1-2\nu_{1o})\mu_2(0)[3K_{2o} + \mu_2(0)] \tag{A13}$$

$$\chi_1 = \frac{b_1 - \sqrt{b_1^2 - 4d_1c_1}}{2d_1} \quad \text{and} \quad \chi_2 = \frac{b_1 + \sqrt{b_1^2 - 4d_1c_1}}{2d_1} \tag{A14}$$

Appendix B

The characteristic equation in the time domain for the elastic/viscoelastic joint shown in Fig. 2 is

$$\begin{aligned}&\eta_1 \sin^2\lambda\pi + 2\eta_2[2\lambda^2\cos^2\gamma - 1]\sin\lambda\pi\sin 2\lambda\gamma - 4\eta_3\lambda^2\sin\lambda\pi\sin 2\lambda\gamma\cos^2\gamma\\ &\quad + 4\eta_4\lambda^2\cos^2\gamma[1 - \cos\lambda\pi\cos 2\lambda\gamma - 2\lambda^2\cos^2\gamma] + \eta_5\left[\sin^2 2\lambda\gamma + 4\lambda^2(\lambda^2-1)\cos^2\gamma - \lambda^4\sin^2 2\gamma\right]\\ &\quad + \eta_6\left\{4\lambda^2\cos^2\gamma[\lambda^2\cos^2\gamma - 1 + \cos\lambda\pi\cos 2\lambda\gamma] + [\cos\lambda\pi - \cos 2\lambda\gamma]^2\right\} = 0\end{aligned} \tag{B1}$$

where

$$\begin{aligned}\eta_1 = &\left[\frac{\mu_{1o}\xi_2}{\xi_1} + 2\mu_2(\infty)(1-\nu_{1o})\right]^2 + \frac{t\exp(\chi_3 t)\mu_{1o}^2(\xi_3\chi_3 + \xi_2/t_o)^2}{\chi_3\xi_4^2}\\ &+ \frac{\exp(\chi_3 t)\mu_{1o}^2(\xi_3\chi_3 + \xi_2/t_o)(\xi_3\chi_3 - \xi_2/t_o)}{\chi_3^2\xi_4^2} + 16\mu_{1o}\mu_2(\infty)(1-\nu_{1o})\exp\left(-\frac{t}{t_o}\right)\\ &+ 4(1-\nu_{1o})^2(\mu_2(0) - \mu_2(\infty))\left[2\mu_2(\infty) + (\mu_2(0) - \mu_2(\infty))\left(1 - \frac{t}{t_o}\right)\right]\exp\left(-\frac{t}{t_o}\right)\\ &+ \frac{4\mu_{1o}(1-\nu_{1o})\exp(\chi_3 t)(\xi_3\chi_3 + \xi_2/t_o)[\chi_3\mu_2(0) + \mu_2(\infty)/t_o]}{\chi_3(\chi_3 + 1/t_o)\xi_4}\end{aligned} \tag{B2}$$

$$\eta_2 = \left[\frac{\mu_{1o}\xi_2}{\xi_1} + 2\mu_2(\infty)(1-\nu_{1o})\right]\left[\frac{\mu_{1o}\xi_2}{\xi_1} - 2\mu_2(\infty)(1-\nu_{1o})\right] + \frac{t\exp(\chi_3 t)\mu_{1o}^2\left(\xi_3\chi_3 + \xi_2/t_o\right)^2}{\chi_3\xi_4^2}$$
$$+ \frac{\exp(\chi_3 t)\mu_1^2\left(\xi_3\chi_3 + \xi_2/t_o\right)\left(\xi_3\chi_3 - \xi_2/t_o\right)}{\chi_3^2\xi_4^2}$$
$$- 4(1-\nu_{1o})^2\left[\mu_2(0) - \mu_2(\infty)\right]\left[2\mu_2(\infty) + \left(\mu_2(0) - \mu_2(\infty)\right)\left(1 - \frac{t}{t_o}\right)\right]\exp\left(-\frac{t}{t_o}\right) \tag{B3}$$

$$\eta_3 = \frac{\mu_2(\infty)}{\xi_1^2}\left[\frac{\mu_{1o}}{\mu_2(\infty)}\xi_2 + 2\xi_1(1-\nu_{1o})\right]\left[3\mu_{1o} - \xi_1(1-2\nu_{1o})\right] + \frac{3\mu_{1o}^2\exp(\chi_3 t)\left[\mu_2(0)\chi_3^2\xi_3 - \mu_2(\infty)\xi_2/t_o^2\right]}{\chi_3^2\xi_4^2}$$
$$+ \frac{3\mu_{1o}^2\exp(\chi_3 t)\left[\mu_2(0)\chi_3 + \mu_2(\infty)/t_o\right]\left(\xi_3\chi_3 + \xi_2/t_o\right)}{\chi_3\xi_4^2} + 2\mu_{1o}\left[\mu_2(0) - \mu_2(\infty)\right](1+\nu_{1o})\exp\left(-\frac{t}{t_o}\right)$$
$$- 2\left[\mu_2(0) - \mu_2(\infty)\right]\left[2\mu_2(\infty) + \left(\mu_2(0) - \mu_2(\infty)\right)\left(1 - \frac{t}{t_o}\right)\right](1-\nu_{1o})(1-2\nu_{1o})\exp\left(-\frac{t}{t_o}\right)$$
$$+ \frac{\mu_{1o}\exp(\chi_3 t)\left\{\left[6\mu_2(0)\chi_3 + \mu_2(\infty)/t_o\right](1-\nu_{1o}) - \left(\xi_3\chi_3 + \xi_2/t_o\right)(1-2\nu_{1o})\right\}\left[\mu_2(0)\chi_3 + \mu_2(\infty)/t_o\right]}{\chi_3\left(\chi_3 + 1/t_o\right)\xi_4} \tag{B4}$$

$$\eta_4 = \frac{\mu_2(\infty)}{\xi_1^2}\left[\frac{\mu_{1o}}{\mu_2(\infty)}\xi_2 - 2\xi_1(1-\nu_{1o})\right]\left[3\mu_{1o} - \xi_1(1-2\nu_{1o})\right] + \frac{3\mu_{1o}^2\exp(\chi_3 t)\left[\mu_2(0)\chi_3^2\xi_3 - \mu_2(\infty)\xi_2/t_o^2\right]}{\chi_3^2\xi_4^2}$$
$$+ \frac{3\mu_{1o}^2 t\exp(\chi_3 t)\left[\mu_2(0)\chi_3 + \mu_2(\infty)/t_o\right]\left(\xi_3\chi_3 + \xi_2/t_o\right)}{\chi_3\xi_4^2} - 2\mu_{1o}\left[\mu_2(0) - \mu_2(\infty)\right](5-7\nu_{1o})\exp\left(-\frac{t}{t_o}\right)$$
$$+ 2\left[\mu_2(0) - \mu_2(\infty)\right]\left[2\mu_2(\infty) + \left(\mu_2(0) - \mu_2(\infty)\right)\left(1 - \frac{t}{t_o}\right)\right](1-\nu_{1o})(1-2\nu_{1o})\exp\left(-\frac{t}{t_o}\right)$$
$$- \frac{\mu_{1o}\exp(\chi_3 t)\left\{\left[6\mu_2(0)\chi_3 + \mu_2(\infty)/t_o\right](1-\nu_{1o}) + \left(\xi_3\chi_3 + \xi_2/t_o\right)(1-2\nu_{1o})\right\}\left[\mu_2(0)\chi_3 + \mu_2(\infty)/t_o\right]}{\chi_3\left(\chi_3 + 1/t_o\right)\xi_4} \tag{B5}$$

$$\eta_5 = \left[\frac{\mu_{1o}\xi_2}{\xi_1} - 2\mu_2(\infty)(1-\nu_{1o})\right]^2 + \frac{t\exp(\chi_3 t)\mu_{1o}^2\left(\xi_3\chi_3 + \xi_2/t_o\right)^2}{\chi_3\xi_4^2}$$
$$+ \frac{\exp(\chi_3 t)\mu_{1o}^2\left(\xi_3\chi_3 + \xi_2/t_o\right)\left(\xi_3\chi_3 - \xi_2/t_o\right)}{\chi_3^2\xi_4^2} - 16\mu_{1o}\left[\mu_2(0) - \mu_2(\infty)\right](1-\nu_{1o})\exp\left(-\frac{t}{t_o}\right)$$
$$+ 4(1-\nu_{1o})^2\left[\mu_2(0) - \mu_2(\infty)\right]\left[2\mu_2(\infty) + \left(\mu_2(0) - \mu_2(\infty)\right)\left(1 - \frac{t}{t_o}\right)\right]\exp\left(-\frac{t}{t_o}\right)$$
$$- \frac{4\mu_{1o}(1-\nu_{1o})\exp(\chi_3 t)\left(\xi_3\chi_3 + \xi_2/t_o\right)\left[\mu_2(0)\chi_3 + \mu_2(\infty)/t_o\right]}{\chi_3\left(\chi_3 + 1/t_o\right)\xi_4} \tag{B6}$$

$$\eta_6 = \mu_2(\infty)\left[\frac{3\mu_1}{\xi_1} - (1-2\nu_{1o})\right]^2 - 6\mu_{1o}\big(\mu_2(0)-\mu_2(\infty)\big)(1-2\nu_{1o})\exp\left(-\frac{t}{t_o}\right)$$
$$+\frac{9t\exp(\chi_3 t)\mu_{1o}^2\big[\mu_2(0)\chi_3+\mu_2(\infty)/t_o\big]^2}{\chi_3\xi_4^2} - \frac{6\mu_{1o}(1-2\nu_{1o})\exp(\chi_3 t)\big[\mu_2(0)\chi_3+\mu_2(\infty)/t_o\big]^2}{\chi_3\big(\chi_3+1/t_o\big)\xi_4}$$
$$+\frac{9\exp(\chi_3 t)\mu_{1o}^2\big[\mu_2(0)\chi_3+\mu_2(\infty)/t_o\big]\big[\mu_2(0)\chi_3-\mu_2(\infty)/t_o\big]}{\chi_3^2\xi_4^2} + (1-2\nu_{1o})^2\big[\mu_2(0)-\mu_2(\infty)\big]$$
$$\times\left[2\mu_2(\infty)+(\mu_2(0)-\mu_2(\infty)\left(1-\frac{t}{t_o}\right)\right]\exp\left(-\frac{t}{t_o}\right)$$
$$-\frac{6\mu_{1o}(1-2\nu_{1o})\exp(\chi_3 t)\big[\mu_2(0)\chi_3+\mu_2(\infty)/t_o\big]^2}{\chi_3\big(\chi_3+1/t_o\big)\xi_4} \tag{B7}$$

$$\xi_1 = 3K_{2o}+\mu_2(\infty);\quad \xi_2 = 3K_{2o}+4\mu_2(\infty);\quad \xi_3 = 3K_{2o}+4\mu_2(0) \tag{B8}$$

$$\xi_4 = 3K_{2o}+\mu_2(0);\quad \chi_3 = -\frac{\xi_1}{\xi_4} \tag{B9}$$

Appendix C

The constant stress field can be expressed in the form $\sigma_{ijo} = \sigma^* F_{ijo}(t)$ where $(i,j) = (r,\theta)$ are plane polar co-ordinates centred at the interface corner, σ^* is one or a combination of the edge loads n_1, n_2, s_1, s_2, and F_{ijo} are non-dimensional constant function of the materials elastic constants, polar co-ordinate θ, and of the joint angle γ. The individual components of the stresses are given by

$$\sigma^1_{rro} = 2(1-\cos 2\theta)M_1 + (\sin 2\theta - 2\theta + \pi\cos 2\theta)M_2 - n_1\cos 2\theta - s_1\sin 2\theta \tag{C1a}$$

$$\sigma^1_{\theta\theta o} = 2(1+\cos 2\theta)M_1 - (2\theta + \sin 2\theta + \pi\cos 2\theta)M_2 + n_1\cos 2\theta + s_1\sin 2\theta \tag{C1b}$$

$$\sigma^1_{r\theta o} = 2\sin 2\theta\cdot M_1 + (1-\pi\sin 2\theta+\cos 2\theta)M_2 + n_1\sin 2\theta - s_1\cos 2\theta \tag{C1c}$$

$$\sigma^2_{rro} = 2(1-\cos 2\theta)N_1 + (\sin 2\theta - 2\theta - \pi\cos 2\theta)N_2 - n_2\cos 2\theta - s_2\sin 2\theta \tag{C1d}$$

$$\sigma^2_{\theta\theta o} = 2(1+\cos 2\theta)N_1 - (2\theta + \sin 2\theta - \pi\cos 2\theta)N_2 + n_2\cos 2\theta + s_2\sin 2\theta \tag{C1e}$$

$$\sigma^2_{r\theta o} = 2\sin 2\theta\cdot N_2 + (1+\pi\sin 2\theta+\cos 2\theta)N_2 + n_2\sin 2\theta - s_2\cos 2\theta \tag{C1f}$$

where the superscript denotes the material number; M_1, M_2, N_1 and N_2 are constant functions which depend on the applied surface tractions, the material properties and the joint angle γ, and are given by,

$$M_1 = n_1\left\{2Q_1\left(\cos^2\gamma+\gamma\sin 2\gamma\right)+2Q_2\left[2\cos^2\gamma+\left(\gamma+\frac{\pi}{2}\right)\sin 2\gamma\right]\cos 2\gamma\right\}$$
$$-n_2\left\{2Q_1\left(\cos^2\gamma+\gamma\sin 2\gamma\right)+2Q_4\left[2\cos^2\gamma+\left(\gamma-\frac{\pi}{2}\right)\sin 2\gamma\right]\cos 2\gamma\right\}$$
$$-s_1\left\{Q_1(\pi-\sin 2\gamma+2\gamma\cos 2\gamma)+\pi Q_3-2Q_4\left[2\cos^2\gamma+\left(\gamma+\frac{\pi}{2}\right)\sin 2\gamma\right]\sin 2\gamma\right\}$$
$$+s_2\left\{Q_1(\pi-\sin 2\gamma+2\gamma\cos 2\gamma)+\pi Q_3-2Q_2\left[2\cos^2\gamma+\left(\gamma-\frac{\pi}{2}\right)\sin 2\gamma\right]\sin 2\gamma\right\} \tag{C2}$$

$$M_2 = 2Q_1(n_1-n_2)\sin 2\gamma-4Q_1(s_1-s_2)\cos^2\gamma \tag{C3}$$

$$N_1 = n_1\left\{2Q_5\left(\cos^2\gamma+\gamma\sin 2\gamma\right)+2Q_4\left[2\cos^2\gamma+\left(\gamma+\frac{\pi}{2}\right)\sin 2\gamma\right]\cos 2\gamma\right\}$$
$$-n_2\left\{2Q_5\left(\cos^2\gamma+\gamma\sin 2\gamma\right)+2Q_2\left[2\cos^2\gamma+\left(\gamma-\frac{\pi}{2}\right)\sin 2\gamma\right]\cos 2\gamma\right\}$$
$$-s_1\left\{Q_5(-\pi-\sin 2\gamma+2\gamma\cos 2\gamma)+\pi Q_3-2Q_4\left[2\cos^2\gamma+\left(\gamma+\frac{\pi}{2}\right)\sin 2\gamma\right]\sin 2\gamma\right\}$$
$$+s_2\left\{Q_5(-\pi-\sin 2\gamma+2\gamma\cos 2\gamma)+\pi Q_3-2Q_2\left[2\cos^2\gamma+\left(\gamma-\frac{\pi}{2}\right)\sin 2\gamma\right]\sin 2\gamma\right\} \tag{C4}$$

$$N_2 = 2Q_5(n_1-n_2)\sin 2\gamma-4Q_5(s_1-s_2)\cos^2\gamma \tag{C5}$$

$$Q_1 = \sum_{i=1}^{3} 4\mu_{1o}(p_i+1/t_o)(\xi_3 p_i+\xi_2/t_o)\exp(p_i t)/Y_i \tag{C6}$$

$$Q_2 = \sum_{i=1}^{5}\frac{8\mu_{1o}(\xi_3 p_i+\xi_2/t_o)(\xi_4 p_i+\xi_1/t_o)\left[\left(\mu_{1o}-\mu_2(0)\right)p_i+\left(\mu_{1o}-\mu_2(\infty)\right)/t_o\right](p_i+1/t_o)\exp(p_i t)}{Z_i} \tag{C7}$$

$$Q_3 = \sum_{i=1}^{5}\frac{32\mu_{1o}(1-\nu_{1o})\left[\mu_2(0)p_i+\mu_2(\infty)/t_o\right](\xi_3 p_i+\xi_2/t_o)^2(p_i+1/t_o)\exp(p_i t)}{Z_i} \tag{C8}$$

$$Q_4 = \sum_{i=1}^{5}\frac{16(1-\nu_{1o})\left[\mu_2(0)p_i+\mu_2(\infty)/t_o\right]\left[\left(\mu_{1o}-\mu_2(0)\right)p_i+\left(\mu_{1o}-\mu_2(\infty)\right)/t_o\right](\xi_4 p_i+\xi_1/t_o)^2\exp(p_i t)}{Z_i} \tag{C9}$$

$$Q_5 = \sum_{i=1}^{3}\frac{8(1-\nu_{1o})(\xi_4 p_i+\xi_1/t_o)\left[\mu_2(0)p_i+\mu_2(\infty)/t_o\right]\exp(p_i t)}{Y_i} \tag{C10}$$

$$p_1 = 0; \quad p_2 = \frac{-S_1 + \sqrt{S_1^2 - 4R_1T_1}}{2R_1}; \qquad p_3 = \frac{-S_1 - \sqrt{S_1^2 - 4R_1T_1}}{2R_1} \tag{C11a}$$

$$p_4 = \frac{-S_2 + \sqrt{S_2^2 - 4R_2T_2}}{2R_2}; \qquad p_5 = \frac{-S_2 - \sqrt{S_2^2 - 4R_2T_2}}{2R_2} \tag{C11b}$$

$$R_1 = 2\mu_{1o}\xi_3\lfloor(\pi - 2\gamma)\sin 2\gamma - 4\cos^2\gamma\rfloor + 4\mu_2(0)\xi_4(1-\nu_{1o})\lfloor(\pi + 2\gamma)\sin 2\gamma + 4\cos^2\gamma\rfloor \tag{C12}$$

$$R_2 = 6\mu_{1o}\mu_2(0) - 2\mu_{1o}\xi_4\cos 2\gamma - \mu_2(0)\xi_4(2 - 4\nu_{1o} - 2\cos 2\gamma) \tag{C13}$$

$$S_1 = \frac{4\mu_{1o}}{t_o}\Big\{\big(\xi_3 - 2\mu_2(0) + 2\mu_2(\infty)\big)\big[(\pi - 2\gamma)\sin 2\gamma - 4\cos^2\gamma\big] + 4(1-\nu_{1o})\big[\mu_2(0)\xi_1 + \mu_2(\infty)\xi_4\big]\big[(\pi + 2\gamma)\sin 2\gamma + 4\cos^2\gamma\big]\Big\} \tag{C14}$$

$$S_2 = \frac{6\mu_{1o}\big(\mu_2(0) + \mu_2(\infty)\big) - 2\mu_{1o}(\xi_1 + \xi_4)\cos 2\gamma - \big(\mu_2(0)\xi_1 + \mu_2(\infty)\xi_4\big)(2 - 4\nu_1 - 2\cos 2\gamma)}{t_o} \tag{C15}$$

$$T_1 = \frac{2\mu_{1o}\xi_1\lfloor(\pi - 2\gamma)\sin 2\gamma - 4\cos^2\gamma\rfloor + 4(1-\nu_{1o})\mu_2(\infty)\xi_1\lfloor(\pi + 2\gamma)\sin 2\gamma + 4\cos^2\gamma\rfloor}{t_o^2} \tag{C16}$$

$$T_2 = \frac{6\mu_{1o}\mu_2(\infty) - 2\mu_{1o}\xi_1\cos 2\gamma - \mu_2(\infty)\xi_1(2 - 4\nu_{1o} - 2\cos 2\gamma)}{t_o^2} \tag{C17}$$

$$Y_1 = 4T_1; \quad Y_2 = 4p_2(2R_1p_2 + S_1); \quad Y_3 = 4p_3(2R_1p_3 + S_1) \tag{C18}$$

$$Z_1 = 4T_1T_2; \qquad Z_2 = 4p_2(2R_1p_2 + S_1)\big(R_2p_2^2 + S_2p_2 + T_2\big) \tag{C19}$$

$$Z_3 = 4p_3(2R_1p_3 + S_1)\big(R_2p_3^2 + S_2p_3 + T_2\big) \tag{C20}$$

$$Z_4 = 4p_4\big(R_1p_4^2 + S_1p_4 + T_1\big)(2R_2p_4 + S_2) \tag{C21}$$

$$Z_5 = 4p_5\big(R_1p_5^2 + S_1p_5 + T_1\big)(2R_2p_5 + S_2) \tag{C22}$$

The parameters ξ_1, ξ_2, ξ_3, and ξ_4 are defined in Eq. (B8).

References

ABAQUS, 1997. Users Manual, version 5.7. HKS Inc.

Akisanya, A.R., Fleck, N.A., 1997. Interfacial cracking from the free-edge of a long bimaterial strip. Int. J. Solids Struct 34, 1645–1665.

Blanchard, J.P., Ghoniem, N.M., 1989. Relaxation of thermal stress singularities in bonded viscoelastic quarter planes. J. Appl. Mech 56, 756–762.

Bogy, D.B., 1970. On the plane problem of edge-bonded elastic quarter planes loaded at the boundary. Int. J. Solids Struct 6, 1287–1313.

Bogy, D.B., 1971. Two edge-bonded elastic wedges of different materials and wedge angles under surface tractions. J. Appl. Mech 38, 377–386.

Christensen, R.M., 1971. Theory of Viscoelasticity — An Introduction. Academic Press, New York.

Delale, R., Erdogan, F., 1981. Viscoelastic analysis of adhesively bonded joints. J. Appl. Mech 48, 331–338.

Dundurs, J., 1969. Mathematical Theory of Dislocations. American Society of Mechanical Engineers, New York.

Fett, T., 1996. Failure of brittle materials near stress singularities. Engng. Fract. Mech 53, 511–518.

Gradin, P.A., 1982. A fracture initiation criterion for edge bonded bi-material bodies. J. Comp. Mater 16, 448–456.

Lee, S.S., 1997. Free-edge stress singularity in a two-dimensional unidirectional viscoelastic laminate model. J. Appl. Mech 64, 408–414.

Lee, S.S., 1998. Boundary element analysis of the stress singularity at the interface corner of viscoelastic adhesive layers. Int. J. Solids Struct 35, 1385–1394.

Liu, D., Fleck, N.A., 1998. Interfacial cracking of scarf joints. Int. J. Fract. (in press).

Miller, M.K., Guy, W.T., 1966. Numerical inversion of the Laplace transform by use of Jacobi polynomials. SIAM J. Numerical Analysis 3, 624–635.

Munz, D., Yang, Y.Y., 1992. Stress singularities at the interface in bonded dissimilar materials under mechanical and thermal loading. J. Appl. Mech 59, 857–861.

Munz, D., Fett, T., Yang, Y.Y., 1993. The regular stress term in bonded dissimilar materials after a change in temperature. Engng. Fract. Mech 44, 185–194.

Qian, Z.Q., Akisanya, A.R., 1999. An investigation of the stress singularity near the free edge of scarf joints. Euro. J. Mech./A-Solids 18, 443–463.

Qian, Z.Q., Akisanya, A.R., 1998a. An experimental investigation of failure initiation in bonded joints. Acta Mater 46, 4895–4904.

Qian, Z.Q., Akisanya, A.R., 1998b. Analysis of free-edge stress and displacement fields in scarf joints subjected to a uniform change in temperature. Fat. Fract. Engng. Mater 21, 687–703.

Reedy, E.D., 1990. Intensity of the stress singularity at the interface corner between a bonded elastic and rigid layer. Engng. Fract. Mech 36, 575–583.

Reedy, E.D., 1993. Asymptotic interface-corner solutions for butt tensile joints. Int. J. Solids Struct 30, 767–777.

Rice, J.R., 1988. Elastic fracture mechanics concepts for interfacial cracks. J. Appl. Mech 55, 98–103.

Sih, G.C., Ho, J.W., 1991. Sharp notch fracture strength characterized by critical energy density. Theor. Appl. Fract. Mech 16, 179–214.

Suh, N.P., 1986. Tribophysics. Prentice-Hall, Englewood Cliffs, NJ.

Wang, S.S., Choi, I., 1982. Boundary layer effects in composite laminates. Part I — Freeedge stress solutions and basic characteristics. J. Appl. Mech 49, 549–560.

Yang, Y.Y., Munz, D., 1995. Stress intensity factor and stress distribution in a joint with an interface corner under thermal and mechanical loading. Comp. Struct 57, 467–476.

Yang, Y.Y., Munz, D., 1997. Stress singularities in a dissimilar materials joint with edge tractions under mechanical and thermal loadings. Int. J. Solids Struct 34, 1199–1216.